THE JOURNAL OF PHYSICAL CHEMISTRY C

Article

pubs.acs.org/JPCC

Monitoring the Electrochemical Processes in the Lithium−Air Battery by Solid State NMR Spectroscopy

Michal Leskes,[†] Amy J. Moore,[†] Gillian R. Goward,[‡] and Clare P. Grey*[,†]

[†]Deparment of Chemistry, University of Cambridge, Lensfield Road, CB2 1EW, Cambridge, United Kingdom

[‡]Department of Chemistry, McMaster University, 1280 Main Street West, Hamilton, Ontario L8S 4M1, Canada

Supporting Information

ABSTRACT: A multi-nuclear solid-state NMR approach is employed to investigate the lithium−air battery, to monitor the evolution of the electrochemical products formed during cycling, and to gain insight into processes affecting capacity fading. While lithium peroxide is identified by ^{17}O solid state NMR (ssNMR) as the predominant product in the first discharge in 1,2-dimethoxyethane (DME) based electrolytes, it reacts with the carbon cathode surface to form carbonate during the charging process. ^{13}C ssNMR provides evidence for carbonate formation on the surface of the carbon cathode, the carbonate being removed at high charging voltages in the first cycle, but accumulating in later cycles. Small amounts of lithium hydroxide and formate are also detected in discharged cathodes and while the hydroxide formation is reversible, the formate persists and accumulates in the cathode upon further cycling. The results indicate that the rechargeability of the battery is limited by both the electrolyte and the carbon cathode stability. The utility of ssNMR spectroscopy in directly detecting product formation and decomposition within the battery is demonstrated, a necessary step in the assessment of new electrolytes, catalysts, and cathode materials for the development of a viable lithium−oxygen battery.

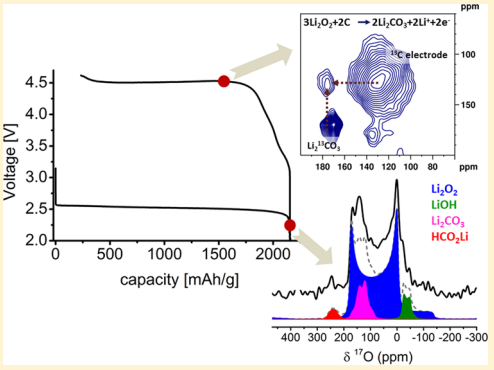

1. INTRODUCTION

The continued increase in global energy consumption and the shift toward electrification of transportation call for significant improvements in current lithium ion battery technology. Such improvements require the design of new materials and new chemistries to enable the development of energy storage devices offering higher energy densities. The lithium air battery is considered a promising candidate for such applications, as it can potentially deliver an order of magnitude higher gravimetric energy density than conventional lithium ion batteries. This high energy is based on the reversible reaction between lithium and oxygen, oxygen being provided from the atmosphere, forming lithium peroxide.[1]

Despite initial results demonstrating reversible cycling of the lithium−oxygen cell using an aprotic electrolyte with capacities of more than 1000 mAh/g,[2] there are several challenges facing the successful development of this battery. Among these are the identification of stable electrolyte salts and solvents, development of inert, porous, and conductive cathode materials, as well as design of catalytic species for reducing the overpotentials of both the discharge and charge processes.[3−5] Several studies have demonstrated and discussed the issue of electrolyte stability in the presence of the highly reactive superoxide species formed during the discharge process. The use of common carbonate solvents was shown to lead to the formation of various electrolyte decomposition products, mostly lithium carbonate.[6−9] Ether solvents, although considered relatively stable in the initial cycles, were shown to decompose upon extended cycling.[10] However, as their use enables the formation of significant amounts of peroxide, tetraethyleneglycol (TEGDME) and 1,2-dimethoxyethane (DME) are used in many studies and are often considered to be relatively inert.[11−13] Other aprotic solvents examined include dimethyl sulfoxide (DMSO) and dimethyl formamide (DMF), which were also shown to decompose to a certain extent.[14−17] Similarly, the stability of the electrolyte salts have been investigated. Studies employing solution nuclear magnetic resonance (NMR) spectroscopy, X-ray diffraction (XRD) and X-ray photoelectron spectroscopy (XPS) have identified that the instability of the lithium salt can reduce the cycle life of the cell due to side reactions that depend strongly on the combination of salt and solvent.[18−21] Much attention has also been given to the porous carbon cathode in the cell. While initially it was thought that the role of the cathode is to mediate the reaction between oxygen and lithium by allowing electron conduction to the site of reaction and housing the reaction products within its pores, recent studies have shown that the carbon cathode itself can affect the morphology and mechanism of the desired reaction product, lithium peroxide.[22] Furthermore, it was suggested that carbonaceous electrodes may not be

Received: October 21, 2013
Revised: November 25, 2013
Published: November 27, 2013

   dx.doi.org/10.1021/jp410429k | J. Phys. Chem. C 2013, 117, 26929−26939

stable in all voltage windows and may be prone to decomposition.[16,23−25]

The carbon stability issues are exacerbated by the large over potentials, and thus higher potentials, associated with the charging process. The charging voltage can, in principle, be lowered by the addition of a catalyst to the electrode formulation and numerous precious metal and metal oxides particles have been proposed as potential catalysts.[26−29] Despite the apparent decrease in charging potential obtained with some of these species, it is becoming increasingly apparent that many of them lead to additional electrolyte decomposition. Furthermore, it remains unclear whether catalysis can take place at all in a system with limited or no solubility of the reaction products.[30]

Clearly the development of a viable lithium-air battery is still at the stage where insight into the electrochemical reactions taking place at the electrode is a necessity. The interplay between the electrode material, the reactants lithium and oxygen, and their products as well as the electrolyte solution must be fully understood so that robust materials can be designed. While new carbon structures, composite electrodes, catalysts, and electrolyte candidates are constantly introduced, their viability and role must be assessed by a careful characterization of the electrochemical processes that they give rise to.

NMR spectroscopy can be particularly enlightening as it allows the detection of the entire bulk of the cathode, detecting both amorphous and ordered phases and provides a thorough description of the electrochemical processes taking place. This contrasts with other analytical tools such as X-ray diffraction, differential mass spectroscopy (DEMS) and surface techniques such as XPS, which focus on smaller fractions of the electrochemical processes: crystalline, gaseous, or surface components respectively.

Although lithium peroxide was shown to form by various techniques such as XRD, secondary emission spectroscopy (SEM), and infrared (IR),[8,25,31,32] its quantification via these methods is not trivial. We have recently shown the strength of ^{17}O ssNMR in investigating this system in part due to the unique NMR parameters of lithium peroxide,[33] demonstrating that the main discharge product in DME is indeed lithium peroxide. However, several other resonances were observed in the ^{17}O spectra of discharged electrodes that were assigned to a series of decomposition products. Here we extend the NMR approach further: by assembling a library of possible reaction products and their NMR signatures we can clearly detect and quantify the amount of lithium peroxide and electrolyte decomposition products formed in working cells.

Since most of the reaction products formed electrochemically contain O and Li, it should be possible to identify them via the acquisition of their ^{6,7}Li and ^{17}O NMR spectra. Although lithium NMR spectra are straightforward to acquire, due to the ionic nature of Li^+ in the (diamagnetic) compounds studied here, the variations between electronic environments in the various compounds are not sufficiently large to cause pronounced differences in chemical shifts.[34] In particular, the lithium peroxide and carbonate chemical shifts differ by only 0.18 ppm[35,36] and hence they are difficult to resolve even when using the lower abundant ^{6}Li nucleus (which generally gives rise to sharper signals due to the weaker homonuclear couplings). ^{17}O, which has a spin 5/2, is a much more sensitive probe to its chemical environment and is therefore the main probe nucleus in this study. The quadrupole coupling constants, C_q, are often of the order of few megahertz, resulting in distinct second order quadrupole line shapes, which, in combination with the chemical shift, allows the identification of most of the electrochemical products formed in the cell.

By performing a multinuclear study of ^{17}O, ^{6,7}Li, ^{1}H, and ^{13}C ssNMR, we identify and quantify the different nonsoluble products formed in the pores and on the surface of the carbon electrode. Furthermore, we monitor the evolution of these products as a function of state of charge and discuss the results in the context of prior mechanistic studies of electrolyte decomposition. Specific carbon-13 labeling of the electrode material and of the electrolyte is used to identify decomposition pathways, and correlation spectroscopy is used to spatially locate the formed species. We expect this approach to be beneficial in evaluating new electrode and electrolytes for lithium−air batteries.

2. EXPERIMENTAL SECTION

a. Electrode Fabrication. Oxygen electrodes were prepared from a mixture of 24 wt % superP Li carbon (Timcal), 38 wt % polyvinylidene fluoride (PVDF) binder, and 38 wt % dibutylphthalate (DBP, Sigma-Aldrich) in acetone. The slurry was then spread into a self-supporting film of thickness 150 μm, cut into disc shape with 1/2″ diameter, and washed with diethyl ether to remove the DBP. The final film contained 40 wt % carbon. The electrodes were then vacuum-dried at 115 °C and taken into an argon filled glovebox without exposure to ambient atmosphere.

^{13}C-enriched electrodes were made following the same procedure using ^{13}C enriched (99%) amorphous carbon powder from Cambridge Isotope Laboratories.

b. Cell Assembly and Electrochemistry. Lithium−oxygen cells were assembled in an argon-filled glovebox using standard 3205 coin cells (Hohsen Corp.) that were modified with 1 mm diameter holes punched to their top case. Cells were assembled by stacking a disc of lithium foil (0.38 mm thickness, Sigma-Aldrich) on top of a stainless steel current collector, followed by a borosilicate glass fiber separator (Whatman). Electrolyte made of 1 M lithium bis(trifluoromethanesulfonyl)-imide (LiTFSI, Sigma Aldrich, vacuum-dried at 250 °C prior to use for 12 h) in 1,2-dimethoxyethane (DME, Sigma Aldrich, vacuum distilled and stored over molecular sieves in an argon glovebox) was added to the separator. The self-supporting carbon electrode was then placed on top, followed by a stainless steel mesh (Advert Materials) and the punched coin cell top. The cell was pressed closed, excess electrolyte removed, and sealed in a glass chamber with two Young valves. Following assembly in the glovebox, cells were flushed with oxygen gas for 30 min through the valves. After adding the oxygen, the cells were rested for 10−20 h and then cycled on an Arbin battery cycler.

Following cycling, cells were disassembled in the glovebox and the cathodes were extracted, washed with anhydrous acetonitrile, and vacuum-dried overnight in the glovebox's prechamber and packed into the NMR rotors without exposure to ambient atmosphere.

For ^{6}Li measurements, ^{6}Li-enriched lithium foil (Cambridge Isotope Laboratories) was used as the anode.

c. ^{17}O Isotope Enrichment. For ^{17}O NMR measurements the cell assembly was performed as described above. Following the addition of natural abundance oxygen, the cell was connected to a vacuum line. ^{17}O enriched oxygen gas (60−70% enrichment, Isotec and Cambridge Isotope Laboratories)

dx.doi.org/10.1021/jp410429k | J. Phys. Chem. C 2013, 117, 26929−26939

was connected to the line. The pressure in the cell was reduced to about 0.8 atm and refilled back to 1 atm with the ^{17}O enriched oxygen gas resulting in about 20−25% ^{17}O enriched oxygen gas. The cell was then rested for 10−20 h and cycled as above.

d. Synthesis of Model Compounds. ^{17}O-enriched LiOH was synthesized following the procedure of Abys et al.[37] from the reaction between n-butyl lithium in hexane (52 mL) and ^{17}O enriched (10%) water (1.5 mL) in 100 mL dry tetrahydrofuran, resulting in 1.5 g of LiOH. ^{17}O-enriched Li_2O was obtained by heating the above LiOH to 700 °C under vacuum, raising the temperature in several steps, again following the procedure by Abys et al.[37] ^{17}O enriched Li_2CO_3 was made by placing the above LiOH in a tube furnace heated to 100 °C and flowing CO_2 gas at a rate of 15 cm^3/min for 12 h. The formation of the phases and their purity was confirmed by X-ray powder diffraction collected on a Panalytical X'Pert Pro diffractometer.

e. Solid State NMR Spectroscopy. ^1H ssNMR measurements were performed on a Bruker 700 MHz Avance III spectrometer using a 1.3 mm double resonance probe. A rotor synchronized Hahn echo sequence was used with a nutation frequency of 120 kHz and a spinning frequency of 60 kHz. The relaxation delay was optimized for each sample with optimal values in the range of 8−12 s. Spectra were referenced to adamantane set at 1.8 ppm. Spectral analysis was performed using the DMFIT software.[38]

^{13}C ssNMR spectra of ^{13}C-enriched cathodes were acquired on a Bruker 300 MHz Avance I spectrometer using a 2.5 mm double resonance probe. A rotor synchronized Hahn echo sequence was used with a nutation frequency of 100 kHz, a spinning frequency of 25 kHz, and a relaxation delay of 20 s. Spectra were referenced to the adamantane tertiary group set at 38.5 ppm. Two dimensional (2D) homonuclear correlation experiments were acquired on a Bruker 400 MHz Avance I spectrometer using a 2.5 mm probe spinning with a spinning frequency of 10 kHz. Radio Frequency Driven Recoupling (RFDR)[39] was used to recouple the dipolar homonuclear interactions using a nutation frequency of 105 kHz for a duration of 200 rotor cycles (20 ms).

$^1H-^6Li$ heteronuclear correlation experiments were performed on a Bruker 700 MHz Avance III spectrometer using a 1.3 mm double resonance probe and a spinning frequency of 60 kHz. Cross-polarization (CP) was used to correlate $^1H-^6Li$ dipolar coupled nuclei with a 5 ms contact time.

^{17}O spectra of discharged cathodes were acquired on a Bruker 850 and 700 MHz Avance III spectrometers using a 1.3 mm probe and a spinning frequency of 60 kHz. A rotor synchronized Hahn echo sequence was used with the highest radio frequency (RF) nutation frequency achieved equal to 91 and 96 kHz on the 700 and 850 MHz spectrometers, respectively). A relaxation delay of 1−1.5 s was used, and the experiment times varied between 20 and 48 h on the 850 MHz spectrometer. The spectra of LiOH and Li_2O were acquired on a Bruker 700 MHz Avance III with a single pulse excitation (nutation frequency of 132 kHz) and a relaxation delay of 5 s. The spectrum of Li_2CO_3 was acquired on a Bruker 850 MHz Avance III spectrometer using a 4 mm double resonance probe using a single pulse excitation (nutation frequency of 42 kHz) with a relaxation delay of 15 s. Natural abundance ^{17}O spectra of anhydrous lithium acetate (CH_3O_2Li) and lithium formate (HCO_2Li) were acquired on a Bruker 900 MHz Avance II spectrometer, using a 4 mm double resonance probe with a rotor synchronized Hahn echo (nutation frequency 42 kHz). A natural abundance ^{17}O spectrum of Li_2O_2 was acquired on a Bruker 850 MHz Avance III spectrometer using a static probe with a solid echo pulse excitation (62 kHz nutation frequency; 30 s relaxation delay). MAS spinning frequencies are specified in the figure captions. Spectra were fit using either SPINEVOLUTION[40] spin dynamics simulation program or the line shape analysis tool in the Bruker software Topspin.

3. RESULTS AND DISCUSSION

a. ^{17}O NMR Spectral Library of Possible Reaction Products. In order to identify the electrochemical products formed in the cathode, we first obtain ^{17}O spectra (Figure 1a−f) and relevant NMR parameters (from fits to the spectra; Table 1) from an assembled library of possible reaction products. For lithium peroxide and carbonate, the fits to the ^{17}O spectra were supported by density functional theory calculations of the NMR parameters, as described in ref 33. As the natural abundance of the ^{17}O isotope is only 0.034%, isotope enrichment was used where possible, and high field measurements were employed for increased sensitivity.

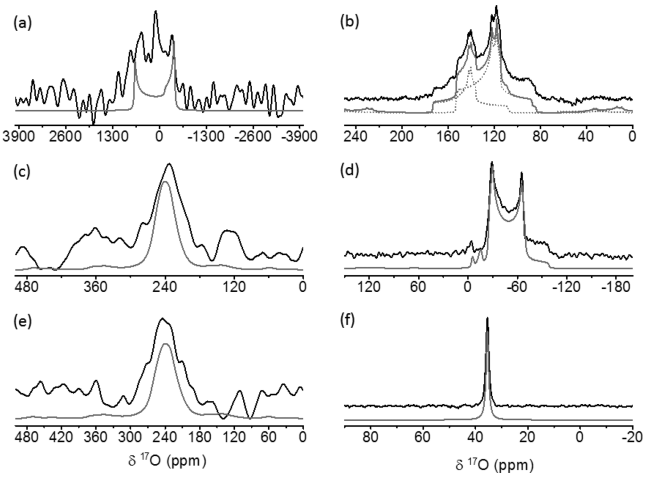

Figure 1. ^{17}O experimental NMR spectra of the various model compounds (black) and simulated best fits (gray) (b−f); the simulated spectrum shown in (a) was calculated using the NMR parameters obtained from ^{17}O-enriched Li_2O_2 obtained electrochemically:[33] (a) Static spectrum of natural abundance Li_2O_2, (b) MAS (12.5 kHz) spectrum of 10% ^{17}O enriched Li_2CO_3, (c) MAS (12.5 kHz) of natural abundance CH_3CO_2Li, (d) MAS (60 kHz) spectrum of 10% ^{17}O enriched LiOH, (e) MAS (12.5 kHz) of natural abundance HCO_2Li, and (f) MAS (60 kHz) spectrum of 10% ^{17}O enriched Li_2O.

The natural abundance spectrum of lithium peroxide (Figure 1a) was acquired without MAS due to the large C_q value expected from ab initio calculations of the NMR parameters.[33] While the low signal-to-noise (S/N) ratio does not allow accurate values of the isotropic chemical shift and quadrupolar coupling to be extracted, the width of this spectrum of more than 2000 ppm in a 20 T field is consistent with the quadrupole singularities calculated with NMR parameters determined from the electrochemically formed lithium peroxide, as shown in our previous work.[33] The large coupling constant (18 MHz), which is more than twice that of most ^{17}O species measured in the solid state,[41] makes it easy to distinguish Li_2O_2 from the other possible products. The relatively sharp resonance between 0 and 200 ppm seen in the natural abundance Li_2O_2 spectrum is due to a lithium carbonate impurity. The two crystallo-

dx.doi.org/10.1021/jp410429k | J. Phys. Chem. C 2013, 117, 26929−26939

Table 1. Experimental and Calculated ^{17}O NMR Parameters of the Various Discharge Products Obtained from the Fits to the Spectra Shown in Figure 1

	δ_{iso}/ppm		$\lvert C_q\rvert$/MHz		η	
compound	experiment	DFT	experiment	DFT	experiment	DFT
Li_2O_2	227	223	18.0 (0.2)*	18.6	0.00 (0.04)	0
Li_2CO_3 (O1)	174	159	7.20 (0.05)	7.4	0.94 (0.05)	0.97
Li_2CO_3 (O2)	154	139	7.40 (0.05)	7.7	0.88 (0.05)	0.91
LiOH	−15		7.05 (0.05)		0.10 (0.1)	
Li_2O	35		0			
HCO_2Li	~265		7.3 (1.6)			
CH_3CO_2Li	~265		7.7 (1.5)			

δ_{iso} is the isotropic chemical shift, C_q is the quadrupole coupling constant, and η is the quadrupole asymmetry parameter. Values in brackets correspond to the error in determining the EFG parameters. *The Li_2O_2 value was extracted from a static spectrum of Li_2O_2 obtained electrochemically.[33]

graphically distinct oxygen sites of lithium carbonate, the most common electrolyte decomposition product, are well resolved in its ^{17}O MAS spectrum (Figure 1b), and can be fit with second order quadrupole line shapes with C_q values of the order of 7.2 and 7.4 MHz. The C_q of another possible decomposition product LiOH (Figure 1d) is similar (7.05 MHz) but its chemical shift is very different, −15 ppm vs 154 and 174 ppm for the carbonate (note that the observed center of masses of these resonances are shifted to higher frequencies from their isotropic chemical shift values due to the second order quadrupolar shift). The natural abundance spectra of lithium acetate and formate (Figure 1c,e) do not have sufficient S/N, even at the high field strength of 21.2 T, to allow accurate determination of their quadrupolar coupling constants. Nevertheless, a C_q value of the order of 7.5 MHz can be used to fit the line width with a chemical shift of the order of 265 ppm, both values lying within the respective ranges reported for carboxyl functional groups.[41] Finally, lithium oxide has been suggested as a discharge product formed in TEGDME electrolytes based on XRD data.[42] No quadrupolar broadening is expected due to the cubic environment of the oxygen sites, and a narrow and well-resolved ^{17}O resonance of Li_2O at 35.6 ppm (Figure 1f) is observed. Thus, if present, its ^{17}O signature can be easily used to identify it in the discharge products. Products containing ether functional groups were not measured, but their ^{17}O resonances are expected to have isotropic shifts in the range of 0−100 ppm with C_q values of the order of 11 MHz.[41]

As the measurements of possible electrochemical products were performed at several different field strengths and with various MAS frequencies, it is not straightforward to compare them with spectra obtained of products formed in an operating battery. Therefore we have simulated the spectra using the parameters listed in Table 1, for all compounds at a single field, 20 T, and spinning frequency, 60 kHz (Figure 2). The simulated spectra demonstrate that high-field ^{17}O MAS spectroscopy is an effective tool for identifying and distinguishing the various oxygen functionalities. Separating between lithium carboxylate groups such as formate and acetate, for example, will, however, require additional ^{1}H and/or ^{13}C measurements.

b. Electrochemistry. In order to identify the products formed in working lithium−oxygen batteries, cells were assembled as described in the Experimental Section. The discharge process was limited by either the discharge capacity (1000 mAh/g; referred to as partial discharge) or by a voltage limitation of 2 V allowing the cell to fully discharge.

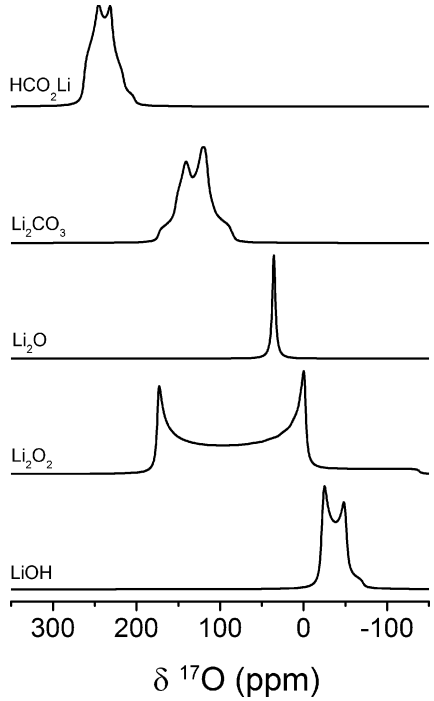

Figure 2. Simulation of the ^{17}O central transition line shape of the various products at 20 T and 60 kHz MAS with the NMR parameters given in Table 1.

Representative electrochemical plots for cells discharged to 1000 mAh/g and with a discharge voltage limit of 2 V are shown in Figure 3. For characterization by ^{17}O NMR, the cells were cycled under an ^{17}O enriched oxygen atmosphere and spectra were obtained following partial and full discharge and on charging to 4.5 V after discharge to a voltage of 2 V. For ^{1}H studies, additional states were investigated as indicated in Figure 3.

c. ^{17}O NMR of Products Formed in Cycled Cathodes. The ^{17}O spectra of the partially and fully discharged and partially charged cathodes are shown in Figure 4a−c along with simulations (fits) of the line shapes using the parameters determined for the possible products formed in the cathode (from Table 1). The main discharge product seen on full discharge (corresponding to a capacity of 2000 mAh/g) is lithium peroxide (Figure 4b), corresponding to approximately 80% of the spectral intensity, on the basis of the spectral simulation. However, the spectra were acquired with a relatively short relaxation delay that is shorter than the longitudinal

dx.doi.org/10.1021/jp410429k | J. Phys. Chem. C 2013, 117, 26929−26939

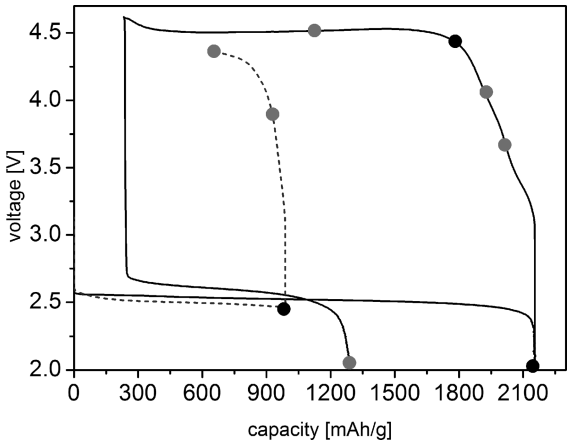

Figure 3. Electrochemical profiles of two representative Li−oxygen cells, one that was limited to a discharge capacity of 1000 mAh/g (dashed gray) and a second cell that was fully discharged to 2 V (black). ^{17}O NMR spectra were acquired for cathodes at the state of charge indicated by black circles and ^{1}H NMR spectra were acquired for those indicated by both black and gray circles.

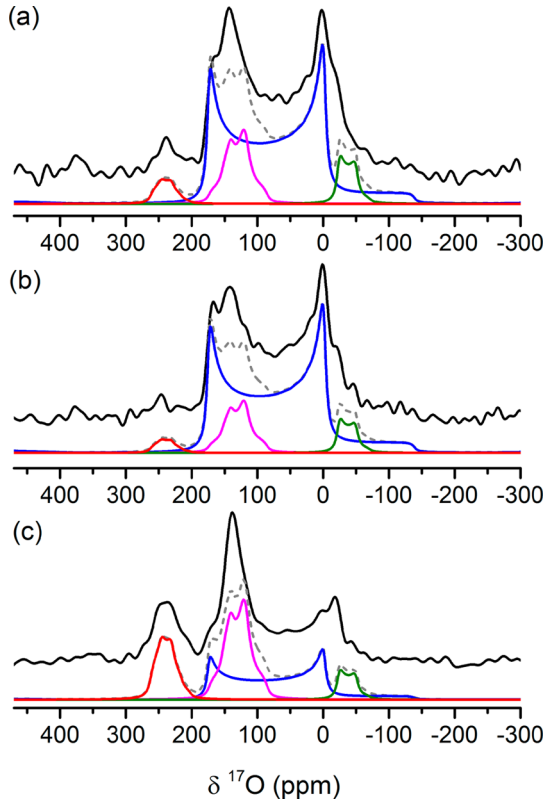

Figure 4. ^{17}O Hahn echo (20 T) spectra of the products formed in cathodes at different state of charge: discharge to 1000 mAh/g (a), discharge to 2 V (b), and discharge to 2 V (capacity of 1650 mAh/g) followed by charge to 4.5 V (capacity of 1070 mAh/g) (c). The experimental spectra (black lines) were simulated (dashed gray) by using the relevant Li_2O_2 (blue), Li_2CO_3 (pink), LiOH (green), and HCO_2Li (red) NMR parameters. The spectra have been scaled so that their heights are equal.

relaxation time, T_1, of the various possible expected products, and thus the actual amount of lithium peroxide is expected to deviate slightly from this value. A detailed analysis of this effect as well as a discussion of the effect of the RF excitation bandwidth and variation in C_q on the relative phase fractions is provided in the Supporting Information. Taking the T_1 relaxation into consideration, the relative amount of lithium peroxide is estimated as 83% with an error of 17% (mainly due to the error in determining the T_1 constant). In addition to the peroxide, a measurable amount of lithium carbonate (5.0 (0.4)%) of the total signal intensity (number in brackets represents the error), lithium hydroxide (10 (5)%) and lithium formate (2.0 (0.2)%) are seen. The resonance at around 260 ppm was assigned to lithium formate and not acetate based on the ^{1}H spectra presented in a later section. The ^{1}H spectra also allow for more accurate quantification of the LiOH concentration. Similar measurements performed at a lower field of 16.4 T could be fit with similar ratios of products (within a few percent) supporting the fits of the 20 T spectra. All the products detected in this ^{17}O measurement must be a result of a reaction between one of the battery components (lithium ions, cathode and electrolyte) with the ^{17}O enriched oxygen gas or one of its ^{17}O-enriched products. It is worth noting that the lithium carbonate and hydroxide resonances do not show the well-defined second order quadrupole line shapes expected from crystalline solids. In the case of the carbonate, similar ^{17}O line shapes were observed in spectra of crystalline carbonate at elevated temperatures due to rotation of the CO_3^{2-} on the microsecond time scale,[43] suggesting that the carbonate ions may be mobile, and possibly indicating the formation of a disordered/amorphous carbonate phase.

The spectrum acquired from a partially discharged cathode (limited to a discharge capacity of 1000 mAh/g) reveals a similar distribution of electrochemical products to that detected at full discharge with Li_2O_2 (80 (17)%), Li_2CO_3 (6.0 (0.5)%), LiOH (12 (6)%), and LiO_2CH (2.0 (0.2)%). Only small differences are seen in the relative concentrations of species, which suggests that these four products are formed simultaneously throughout the discharge process rather than forming at different times during the discharge. Thus, despite the improved cycling performance achieved when limiting the depth of discharge,[4,44] a similar extent of electrolyte decomposition is observed (relative to peroxide formation) for partial and full discharge.

The ^{17}O spectrum of the fully discharged and then charged to 4.5 V cathode (Figure 4c) shows that a large amount of the peroxide has decomposed, decreasing in relative contribution to 56 (13)%, with lithium carbonate now corresponding to 16 (2)% of the total spectral intensity, hydroxide to 15 (8)%, and formate to about 13 (1)%. Thus, as the voltage increases to 4.5 V, most, but not all, of the lithium peroxide has been decomposed. (A method to allow the spectral intensity of the three different spectra to be compared is discussed later.) Previous studies have shown that carbon cathodes preloaded with lithium peroxide exhibited a charge voltage of 4.15 V, leading to almost full removal of the lithium peroxide.[45] Our results indicate that indeed some of the peroxide was removed at lower voltages but the formation of additional decomposition products must increase the overpotential of the charge process beyond 4 V. This is consistent with DEMS measurements performed following the discharge of lithium−oxygen cells where mostly O_2 evolution was detected on charge below 4 V vs lithium, while significant CO_2 release was observed at higher charging potentials between 4 and 4.5 V.[22,23]

In summary, ^{17}O NMR measurements reveal that the main electrochemical product in the first discharge is lithium peroxide, but with a non-negligible contribution from the

dx.doi.org/10.1021/jp410429k | J. Phys. Chem. C 2013, 117, 26929−26939

^{17}O-enriched decomposition products lithium carbonate, hydroxide, and formate and/or acetate.

d. ^{1}H ssNMR of Cycled Cathodes. To monitor the hydrogen containing species, ^{1}H Hahn-echo NMR spectra were acquired from cathodes extracted from cells cycled to various stages (Figure 3). The spectra are dominated by a resonance at 2.6 ppm, which corresponds to the PVDF binder in the cathode. Examining first cells that were fully discharged (Figure 5a), we can identify two main products: a broad peak in the range −1.0 to −1.5 ppm assigned to LiOH, and a weaker resonance at 8 ppm assigned to lithium formate. Another resonance can be resolved at about 0.5 ppm, which will be discussed shortly. As the cells are charged, the LiOH and 0.5 ppm peak decrease in intensity until they almost completely disappear when the cell is half charged (charge capacity of 1000 mAh/g). The formate peak intensity on the other hand does not change noticeably as the cell is charged and is still present at midcharge. In the spectrum of the cell following the second discharge (top row; D2v-C4.65-D2v) the intensity of all the signals grow, indicating that even more significant decomposition occurs with further cell cycling.

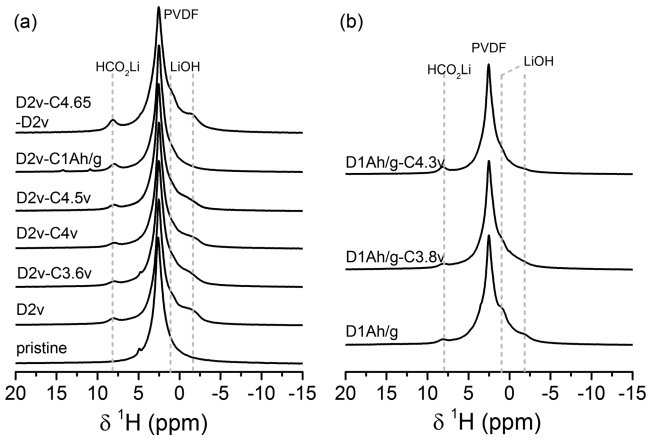

Figure 5. ^{1}H Hahn echo spectra of cathodes at different states of charge following (a) full discharge to 2 V and (b) partial discharge to 1000 mAh/g. Spectra are labeled according to the state of charge, where D and C stand for discharge and charge, respectively, and either the voltage or capacity limit are specified. Spectra have been normalized to the intensity of the PVDF resonance, which is assumed to be constant.

Spectra acquired from cells that were stopped at partial discharge (Figure 5b) display similar ^{1}H resonances with lithium hydroxide resonating in the range of −1.5 to 1 ppm and lithium formate at 8 ppm. The main difference observed with depth of discharge is the disappearance of the LiOH resonance at lower charging voltages, (4.3 V for partially discharged cathodes as compared with 4.5−4.6 V for cathodes that were fully discharged). This difference can be ascribed to the thinner layer of insulating products formed on the cathode surface at partial discharge, which leads to a lower overpotential on charge.

The PVDF signal, although useful as a reference for quantifying the amounts of products formed, obscures any additional weaker resonances with chemical shifts in a similar shift range, for example, lithium acetate (1.9 ppm), lithium methoxide (3.5 ppm), and other possible ether fragments (approximately, 3 ppm). These resonances can potentially be identified by subtracting the pristine cathode spectrum from that of the cycled ones, allowing the signal at around 0.5 ppm to be resolved more clearly and an additional resonance at 3.5 ppm can be identified in the spectra of the partially discharged cells (Figure S5, Supporting Information). Further support for the presence of these signals is provided by a ^{1}H−^{6}Li correlation NMR spectra acquired from a cathode discharged to 1000 mAh/g vs ^{6}Li metal to form ^{6}Li-enriched electrochemical products (Figure 6). This experiment allows signals from protons and ^{6}Li nuclei in close spatial proximity to be correlated by using cross-polarization (CP)[46] for magnetization transfer from ^{1}H to ^{6}Li, and it therefore selects products that contain both nuclei in close proximity. Although the various species cannot be resolved in the ^{6}Li dimension, four species can be clearly resolved in the ^{1}H projection: lithium formate at 8 ppm, lithium hydroxide at −1 ppm and the two additional environments at 3.5 ppm and 0.5 ppm. Based on solution NMR measurements of cathodes washed with D_2O (Figure S6, Supporting Information), we assign the 3.5 ppm peak to the dilithium salt formed from the central fragment of DME, $LiOCH_2CH_2OLi$. This signal is observed in significant amounts only in cathodes that were partially discharged to 1000 mAh/g and for cathodes that were only partially charged after this partial discharge. It disappears on charging to 4.3 V (Figure S5, Supporting Information). Its absence from the 1D difference and 2D heteronuclear correlation spectra of cathodes that were fully discharged suggests that this dilithium salt reacts further as the discharge process proceeds, possibly oxidizing to lithium formate and lithium hydroxide (see below). The 0.5 ppm environment is assigned to a disordered lithium hydroxide phase: while crystalline, stoichiometric lithium hydroxide gives rise to ^{1}H resonance at −1.4 ppm (Figure S7a, Supporting Information); the hydroxide signals detected from the cathode span −1 to 1 ppm. This shift in resonance frequency is tentatively assigned to the disorder in the hydroxide phase. To confirm this assignment, we monitored the ^{7}Li signal build up in a cross-polarization experiment as a function of the cross-polarization time from surrounding protons (Figure S7c). The similar time scale of the build up rate of the signals at −1 and

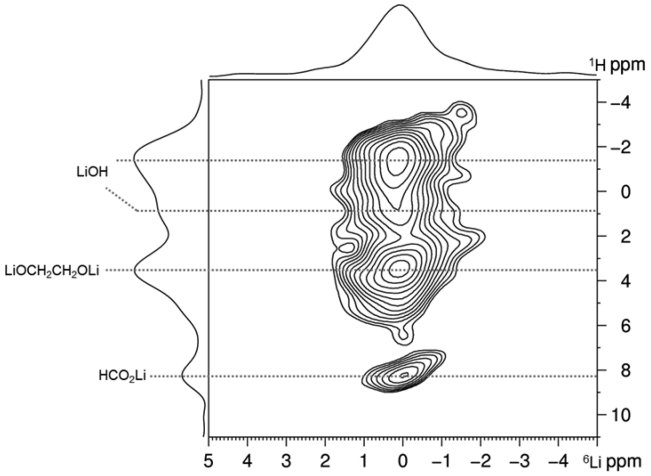

Figure 6. ^{1}H−^{6}Li 2D heteronuclear correlation of a cathode discharged to 1000 mAh/g. The spectrum was acquired at 16.4 T (^{1}H Larmor frequency 700 MHz) at 60 kHz MAS using a 5 ms cross-polarization time to transfer magnetization from ^{1}H (vertical) to ^{6}Li (horizontal) spectra nuclei.

dx.doi.org/10.1021/jp410429k | J. Phys. Chem. C 2013, 117, 26929−26939

0.5 ppm confirms they belong to phases that are structurally similar at least on a short length-scale.

The ^{1}H ssNMR measurements are consistent with the ^{17}O spectra, showing the formation of lithium hydroxide upon cathode discharge and its full removal during the charging process. In addition, lithium formate, which has been detected in former studies,[31] is shown here to accumulate in the cathode upon cycling. The 1,2-ethanediol lithium salt is observed at partial discharge, but it then decomposes on charging the cell to 4.3 V. It has almost completely disappeared in a cathode allowed to fully discharge.

e. ^{13}C ssNMR of ^{13}C Enriched Cathodes. In order to identify the sources of lithium carbonate formation, cells were cycled with cathodes that were prepared with ^{13}C enriched amorphous carbon. While these cathodes may differ in their performance from that of superP Li carbon (due to differences in properties such as the nature of the surface groups, particle sizes and surface area), they are used here to investigate the carbon stability in the relevant electrochemical window. A representative electrochemical profile is shown in Figure S8 in the Supporting Information.

The ^{13}C MAS spectra (Figure 7) all contain the signal of the bulk electrode at 130 ppm, a typical shift position for an sp^2 hybridized carbon. As the cell is fully discharged, a new weak carbon resonance appears at 168 ppm corresponding to lithium carbonate. Upon charge, the carbonate signal grows noticeably, but is completely removed at full charge when a voltage of just over 4.5 V is reached. Significantly larger quantities of carbonate are formed on the second discharge and accumulate on the cathode by the end of two cycles. On the fifth discharge, the amount of carbonate formed corresponds to about 9% of the total carbon signal detected.

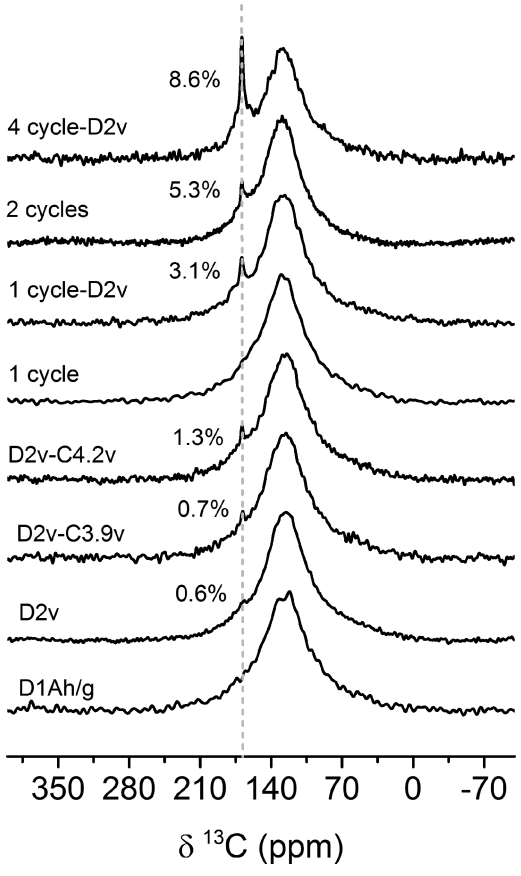

Figure 7. ^{13}C Hahn echo MAS NMR spectra acquired from cycled ^{13}C enriched cathodes. The position of the carbonate group of Li_2CO_3 is indicated via gray dashes, along with its integrated intensity relative to the total carbon signal.

Since a lithium carbonate signal is not detected when using the natural abundance (nonenriched) carbon electrode, for similar experimental parameters (and direct excitation of the ^{13}C resonances), the carbonate signal detected in these measurements must be enriched in ^{13}C and thus originate from the decomposition of the carbon electrode rather than the aprotic solvent. This signal should be contrasted with the carbonate signal detected in the ^{17}O spectra that can originate from the electrolyte or carbon cathode or both. One possibility, supported by prior DEMS, FTIR, and carbonate dissolution reactions also using ^{13}C enriched electrodes,[16,24] is that the carbonate is formed from the reaction between lithium peroxide and the carbon electrode, especially at the higher voltages reached during charge.

To investigate the location of the carbonate species, a ^{13}C homonuclear correlation experiment was performed (Figure 8),

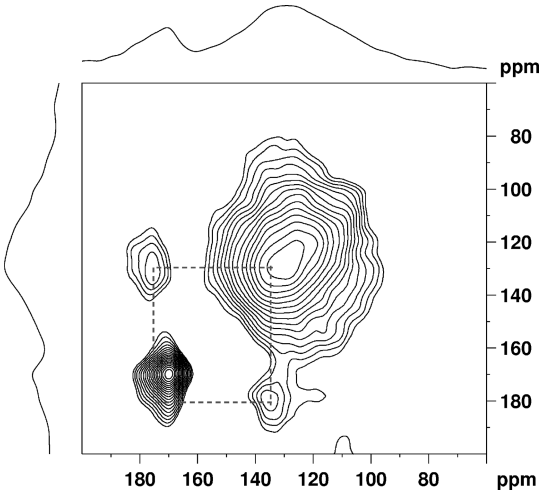

Figure 8. ^{13}C−^{13}C 2D homonuclear correlation of a ^{13}C carbon enriched cathode on its 5th discharge to 2 V. The spectrum was acquired at 9.4 T (Larmor frequency 100 MHz), with 10 kHz MAS, and an RFDR mixing time of 20 ms.

which allows us to detect spatial proximity between ^{13}C sites. A homonuclear correlation was detected between the lithium carbonate resonance at 168 ppm, and the carbon electrode signal at 130 ppm, which shows that at least some of the lithium carbonate forms directly (within a few angstroms) on the surface of the carbon electrode and not on top of the layer of peroxide in contact with the electrolyte. This result is consistent with the observed ^{13}C enriched carbonate being a product of the reaction between the electrode and lithium peroxide. Interestingly, the ^{13}C signal of the carbonate signal nearby the carbon electrode that gives rise to the cross-peaks is at a slightly higher frequency than the sharp carbonate signal. The shift is tentatively ascribed to electronic effects due to the interaction with the carbon electrode and/or the disorder of the carbonate at this interface.

Measurements were also performed using DME 20% ^{13}C-enriched on the methyl group. No ^{13}C signal could be detected from fully discharged cathodes in experiments using direct excitation of ^{13}C resonances, and ^{1}H to ^{13}C and ^{7}Li to ^{13}C CP

dx.doi.org/10.1021/jp410429k | J. Phys. Chem. C 2013, 117, 26929−26939

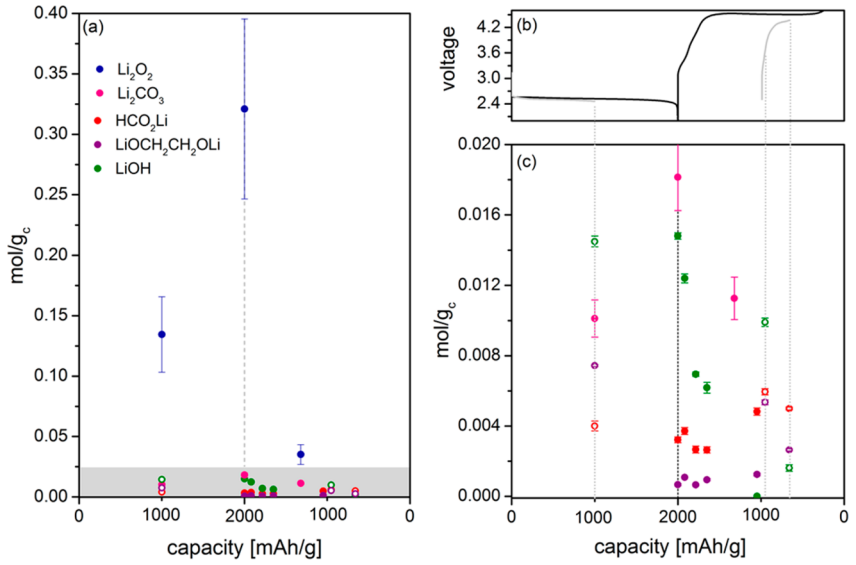

Figure 9. Summary of the products formed in the first cycle of the cell in moles per gram of carbon electrode: Li_2O_2 (blue), Li_2CO_3 (pink), LiOH (green), HCO_2Li (red), and $(LiOCH_2)_2$ (purple). Data collected from cathodes with a discharge limit of 2 V is given by filled circles and a limit of 1000 mAh/g in open circles. The whole range is shown in (a) and an enlargement of the gray area is plotted in (c). Representative voltage profiles are shown in (b).

experiments, indicating that the electrolyte decomposition products formed from the CH_3 group of DME (formate and carbonate) are present in too low concentrations to be detected over the natural abundance carbon signal. A weak signal from the lithium formate could be detected in a ^1H to ^{13}C CP spectrum at the end of the second discharge, consistent with the ^1H NMR experiments, which show that this species accumulates on cycling. Further experiments are in progress using DME with higher ^{13}C enrichment levels to obtain spectra with better signal-to-noise.

f. Summary of Electrochemical Reactions in the First Cycle in DME. We can now combine all of the information collected from various NMR measurements described above and estimate the extent of formation and decomposition of the various detected products (Figure 9). The quantities of lithium hydroxide, formate, and 1,2-ethanediol lithium salt are based on the ^1H spectra where the PVDF signal was used as internal reference. The relative lithium peroxide and carbonate amounts were extracted from the ^{17}O data (correcting for the relaxation effect as discussed in the Supporting Information) and were determined by comparing their relative signal intensity to that of the ^{17}O signals of the protonated species lithium formate. Due to the relatively large error in determining the amount of lithium hydroxide from the ^{17}O NMR data, only ^1H spectra were used to quantify its formation.

At partial discharge (limited to 1000 mAh/g), five products can be identified: lithium peroxide as the major product, and four decomposition products, LiOH, lithium formate, lithium carbonate and the 1,2-ethanediol lithium salt. The decomposition pathway of ether solvents has been discussed in several publications.[10,47−49] While it is mostly agreed that lithium peroxide is formed on discharge by a two-step process,[50]

$$O_2 + Li^+ + e^- \rightarrow LiO_2 \quad \text{(i)}$$

$$2LiO_2 \rightarrow Li_2O_2 + O_2 \text{ or } LiO_2 + Li^+ + e^- \rightarrow Li_2O_2 \quad \text{(ii)}$$

several possibilities have been raised for the mechanism for the decomposition of the ether electrolyte, which differ in the nature of the attacking group. Among the suggestions are reactions involving the superoxide ion and molecular oxygen,[10,51] autoxidation by molecular oxygen,[52] and reactions with the peroxide product.[48,53] DEMS and coulometry measurements have shown that the electron to oxygen ratio (e^-/O_2) consumed in the discharge reaction in DME based electrolytes is always larger than two.[24] Since two electrons are required for the formation of lithium peroxide, it was concluded that any parasitic reactions involving the electrolyte are probably due to the reactivity of the strong nucleophile Li_2O_2 (and not the intermediate LiO_2).[24] DFT calculations performed by Bryantsev et al. have demonstrated that it is unlikely that DME decomposition is initiated by nucleophilic attack of the superoxide ion, these calculations being supported by reactivity tests of DME with KO_2.[54] DME decomposition pathways by reaction with solid lithium peroxide are supported by the high reactivity of the peroxide surface groups.[55] However, several mechanistic pathways can occur, resulting in different decomposition products. Recent computational studies have shown that hydrogen abstraction from the methylene group of DME is energetically favorable, assuming reactivity of single oxygen bridging sites on the surface of the peroxide species.[49] An experimental study based on in situ electrochemical quartz crystal microbalance (EQCM), solution phase NMR, and matrix-assisted laser desorption/ionization time-of-flight (MALDI-TOF) measurements ascribed the reactivity in triglyme electrolytes to the peroxide anion (LiO_2^-) species formed prior to precipitation of the solid Li_2O_2.[48]

Some plausible reactions for the formation of the observed products in the current study (with ^{17}O enriched O_2) are

$$CH_3{-}OCH_2CH_2O{-}CH_3 + 2Li_2{}^{17}O_2 \rightarrow 2CH_3{}^{17}O{}^{17}OLi + LiOCH_2CH_2OLi \quad \text{(iii)}$$

$$CH_3OOLi + 1/2O_2 \rightarrow HCO_2Li + H_2O \quad \text{(all O atoms enriched in } {}^{17}O) \quad \text{(iv)}$$

dx.doi.org/10.1021/jp410429k | J. Phys. Chem. C 2013, 117, 26929−26939

$$Li_2O_2 + H_2O \rightarrow 2LiOH + 1/2O_2$$
(all O atoms enriched in ^{17}O) (v)

$$LiOCH_2CH_2OLi + Li_2{}^{17}O_2 + 2{}^{17}O_2 \rightarrow 2Li_2C{}^{17}O_2O + 2H_2{}^{17}O \quad \text{(vi)}$$

$$HCO_2Li + Li_2O_2 \rightarrow Li_2CO_3 + LiOH$$
(all O atoms enriched in ^{17}O) (vii)

$$C + Li_2O_2 + 1/2O_2 \rightarrow Li_2CO_3$$
(all O atoms enriched in ^{17}O) (viii)

The formation of the diglyme lithium salt, $LiOCH_2CH_2OLi$, at partial discharge (eq iii), which is only detected by ^1H NMR and not by ^{17}O NMR spectroscopy, supports the mechanisms suggested by Aurbach et al., involving a reaction between the peroxide and the DME α-carbon (reaction path b, Scheme 2 in ref 48). Presumably, the methylperoxy lithium product formed in reaction iii, CH_3OOLi, is not detected in our study, because it is readily oxidized to lithium formate (reaction iv) via formaldehyde as an intermediate. Reaction iv also forms water, which can react further to form LiOH (reaction v). Note that the decomposition of one molecule of DME results, via these reactions, in two molecules of water and four molecules of LiOH, helping to explain why LiOH is a dominant product on discharge. On deeper discharge, the diglyme lithium salt has a lower concentration, presumably due to its further reaction to form other lithium salts such as carbonate (reaction vi), hydroxide and formate. Formate is present throughout (in low concentrations) as it is both a product and a reactant in the decomposition pathways suggested above. The reaction of the carbon electrode to form lithium carbonate (reaction viii) is not significant on the first discharge, as very little carbonate is seen in the ^{13}C spectra of ^{13}C enriched electrodes at this stage, consistent with the DEMS and FTIR study of Thotiyl et al.[16] Upon charge, the lithium hydroxide gradually decomposes and is completely removed when the voltage increases up to 4.5 V. Lithium peroxide is decomposed, partially in a reversible manner to release O_2 and to a lesser extent by reacting with the carbon electrode to form lithium carbonate (as detected by ^{13}C NMR):

$$2C + 3Li_2O_2 \rightarrow 2Li_2CO_3 + 2e^- + 2Li^+ \quad \text{(ix)}$$

This reaction produces only two electrons from three peroxide molecules (as compared to six electrons for full oxidation of the peroxide). While the lithium peroxide accounts for about 80% of the discharge capacity (1600 mAh/g), on the basis of the total capacity and the Li_2O_2:decomposition products ratio, its signal intensity observed in the ^{17}O spectrum quickly drops by about 80% when the cell is charged from 2 to 4.5 V with a charge capacity of only about 500 mAh/g. Oxidation of the carbon electrode can at least partially explain this fast decrease in peroxide intensity, the decomposition of Li_2CO_3 at 4.5 V, and above releasing the residual four electrons (from the original three peroxide anions):

$$2Li_2CO_3 \rightarrow 2CO_2 + O_2 + 4e^- + 4Li^+ \quad \text{(x)}$$

Although essentially all the carbonate decomposes at higher voltages in the first cycle, in subsequent cycles, this is not complete (as observed by ^{13}C NMR). Interestingly, the 2D ^{13}C NMR spectrum of the ^{13}C enriched discharged electrode after five cycles shows two types of carbonate signals: one nearby the carbon, and a sharper resonance that is further from the carbon (i.e., it does not give rise to a carbon−carbonate cross peak) and is less disordered. It is likely that it is this latter carbon that is more difficult to decompose electrochemically on charge and gradually accumulates on cycling. Finally, in contrast to the carbonate, lithium formate, which is mainly formed upon discharge, maintains an essentially constant level and is not removed upon charge. The accumulation of the formate and at a later stage lithium carbonate may be one cause of the capacity fading observed in operating cells.

4. CONCLUSIONS

The electrochemical products formed upon cycling of lithium−oxygen cells in 1 M LiTFSI in DME have been identified and monitored using solid state NMR. While lithium peroxide is identified as the main discharge product, non-negligible electrolyte decomposition is detected already at capacities of 1000 mAh/g. The formation of peroxide and decomposition products continues until the end of discharge where additional carbonate formation is detected from the reaction between peroxide and the carbon electrode. ^{13}C homonuclear correlation experiments reveal the formation of carbonate directly on the electrode surface and provide evidence for the carbon electrode reactivity. Upon charge, significant decomposition of lithium peroxide occurs at voltages below 4 V to form oxygen and via a significant electrochemical reaction with the electrode to form lithium carbonate. Lithium hydroxide is removed at voltages, lower than 4.5 V, while for complete removal of the carbonate voltages higher than 4.5 V are required. Lithium formate does not completely decompose under the conditions used here and it accumulates on the cathode. Upon further cycling, additional electrolyte decomposition occurs, resulting in the accumulation of lithium salts on the carbon surface leading to capacity fading and increased overpotentials.

Solid state NMR, in particular ^{17}O NMR, is demonstrated to be a valuable tool in the assessment of lithium−air cells and is expected to be useful in the evaluation of the functionality of new cell components such as electrolytes, electrode materials, and catalytic species.

■ ASSOCIATED CONTENT

Ⓢ Supporting Information

Further details on the analysis of the ^{17}O NMR data; additional experimental results supporting ^1H spectra assignment; electrochemical performance of ^{13}C enriched electrodes. This material is available free of charge via the Internet at http://pubs.acs.org.

■ AUTHOR INFORMATION

Corresponding Author

*E-mail: cpg27@cam.ac.uk; phone: +44 (0)1223 336539.

Notes

The authors declare no competing financial interest.

■ ACKNOWLEDGMENTS

The UK 850 MHz Solid-State NMR Facility used in this research was funded by EPSRC and BBSRC, as well as by the University of Warwick with partial funding through Birmingham Science City Advanced Materials Projects 1 and 2 supported by Advantage West Midlands (AWM) and the

European Regional Development Fund (ERDF). We also thank the National Ultrahigh-Field NMR Facility for Solids (Ottawa, Canada), a national research facility funded by the Canadian Foundation for Innovation, the Ontario Innovation Trust, and Recherche Quebec, for access to the 900 MHz NMR spectrometer. We thank Prof. Dominic Wright and Matthew Dunstan for their help in synthesizing the ^{17}O enriched compounds and Prof. Peter Bruce and Timothy King for helpful discussions. M.L is an awardee of the Weizmann Institute of Science – National Postdoctoral Award for Advancing Women in Science and thanks the EU Marie Curie intra-European fellowship for funding. We thank Johnson Matthey for funding (A.J.M.) and fruitful discussions. This research was supported by the Engineering and Physical Sciences Research Council as part of the Supergen energy storage consortium.

REFERENCES

(1) Bruce, P. G.; Freunberger, S. A.; Hardwick, L. J.; Tarascon, J. M. Li-O_2 and Li-S Batteries with High Energy Storage. *Nat. Mater.* **2012**, *11*, 19–29.

(2) Ogasawara, T.; Débart, A.; Holzapfel, M.; Novák, P.; Bruce, P. G. Rechargeable LI_2O_2 Electrode for Lithium Batteries. *J. Am. Chem. Soc.* **2006**, *128*, 1390–3.

(3) Girishkumar, G.; McCloskey, B.; Luntz, a. C.; Swanson, S.; Wilcke, W. Lithium–Air Battery: Promise and Challenges. *J. Phys. Chem. Lett.* **2010**, *1*, 2193–2203.

(4) Christensen, J.; Albertus, P.; Sanchez-Carrera, R. S.; Lohmann, T.; Kozinsky, B.; Liedtke, R.; Ahmed, J.; Kojic, A. A Critical Review of Li/Air Batteries. *J. Electrochem. Soc.* **2012**, *159*, R1.

(5) Garcia-Araez, N.; Novák, P. Critical Aspects in the Development of Lithium–air Batteries. *J. Solid State Electrochem.* **2013**, *17*, 1793–1807.

(6) Mizunu, F.; Nakanishi, S.; Kotani, Y.; Yokoishi, S.; Iba, H. Rechargeable Li–Air Batteries with Carbonate-Based Liquid Electrolytes. *Electrochemistry* **2010**, *No. 5*, 78.

(7) Freunberger, S. a; Chen, Y.; Peng, Z.; Griffin, J. M.; Hardwick, L. J.; Bardé, F.; Novák, P.; Bruce, P. G. Reactions in the Rechargeable Lithium–O_2 Battery with Alkyl Carbonate Electrolytes. *J. Am. Chem. Soc.* **2011**, *133*, 8040–7.

(8) McCloskey, B. D.; Bethune, D. S.; Shelby, R. M.; Girishkumar, G.; Luntz, A. C. Solvents' Critical Role in Nonaqueous Lithium–Oxygen Battery Electrochemistry. *J. Phys. Chem. Lett.* **2011**, *2*, 1161–1166.

(9) Xu, W.; Xu, K.; Viswanathan, V. V; Towne, S. A.; Hardy, J. S.; Xiao, J.; Nie, Z.; Hu, D.; Wang, D.; Zhang, J. Reaction Mechanisms for the Limited Reversibility of Li–O_2 Chemistry in Organic Carbonate Electrolytes. *J. Power Sources* **2011**, *196*, 9631–9639.

(10) Freunberger, S. a; Chen, Y.; Drewett, N. E.; Hardwick, L. J.; Bardé, F.; Bruce, P. G. The Lithium-Oxygen Battery with Ether-Based Electrolytes. *Angew. Chem., Int. Ed. Engl.* **2011**, 1–6.

(11) Lu, Y.; Kwabi, D. G.; Yao, K. P. C.; Harding, J. R.; Zhou, J.; Zuin, L.; Shao-Horn, Y. The Discharge Rate Capability of Rechargeable Li–O_2 Batteries. *Energy Environ. Sci.* **2011**, *4*, 2999.

(12) Lu, Y.-C.; Gallant, B. M.; Kwabi, D. G.; Harding, J. R.; Mitchell, R. R.; Whittingham, M. S.; Shao-Horn, Y. Lithium–Oxygen Batteries: Bridging Mechanistic Understanding and Battery Performance. *Energy Environ. Sci.* **2013**, *6*, 750.

(13) Jung, H.; Hassoun, J.; Park, J.; Sun, Y.; Scrosati, B. An Improved High-Performance Lithium–Air Battery. *Nat. Chem.* **2012**, *4*, 579–85.

(14) Read, J.; Mutolo, K.; Ervin, M.; Behl, W.; Wolfenstine, J.; Driedger, a.; Foster, D. Oxygen Transport Properties of Organic Electrolytes and Performance of Lithium/Oxygen Battery. *J. Electrochem. Soc.* **2003**, *150*, A1351.

(15) Xu, D.; Wang, Z.; Xu, J.; Zhang, L.; Zhang, X. Novel DMSO-Based Electrolyte for High Performance Rechargeable Li-O_2 Batteries. *Chem. Commun. (Cambridge, U. K.)* **2012**, *48*, 6948–50.

(16) Ottakam Thotiyl, M. M.; Freunberger, S. a; Peng, Z.; Bruce, P. G. The Carbon Electrode in Nonaqueous Li-O_2 Cells. *J. Am. Chem. Soc.* **2013**, *135*, 494–500.

(17) Chen, Y.; Freunberger, S. a; Peng, Z.; Bardé, F.; Bruce, P. G. Li–O_2 Battery with a Dimethylformamide Electrolyte. *J. Am. Chem. Soc.* **2012**, *134*, 7952–7.

(18) Veith, G. M.; Dudney, N. J. Current Collectors for Rechargeable Li–Air Batteries. *J. Electrochem. Soc.* **2011**, *158*, A658.

(19) Nasybulin, E.; Xu, W.; Engelhard, M. H.; Nie, Z.; Burton, S. D.; Cosimbescu, L.; Gross, M. E.; Zhang, J. Effects of Electrolyte Salts on the Performance of Li–O_2 Batteries. *J. Phys. Chem. C* **2013**, *117*, 2635–2645.

(20) Du, P.; Lu, J.; Lau, K. C.; Luo, X.; Bareño, J.; Zhang, X.; Ren, Y.; Zhang, Z.; Curtiss, L. a; Sun, Y.-K.; et al. Compatibility of Lithium Salts with Solvent of the Non-Aqueous Electrolyte in Li–O_2 Batteries. *Phys. Chem. Chem. Phys.* **2013**, *15*, 5572–81.

(21) Younesi, R.; Hahlin, M.; Treskow, M.; Scheers, J.; Johansson, P.; Edström, K. Ether Based Electrolyte, $LiB(CN)_4$ Salt and Binder Degradation in the Li–O_2 Battery Studied by Hard X-ray Photoelectron Spectroscopy (HAXPES). *J. Phys. Chem. C* **2012**, *116*, 18597–18604.

(22) Gallant, B. M.; Mitchell, R. R.; Kwabi, D. G.; Zhou, J.; Zuin, L.; Thompson, C. V.; Shao-Horn, Y. Chemical and Morphological Changes of Li–O_2 Battery Electrodes Upon Cycling. *J. Phys. Chem. C* **2012**, *116*, 20800–20805.

(23) McCloskey, B. D.; Speidel, A.; Scheffler, R.; Miller, D. C.; Viswanathan, V.; Hummelshøj, J. S.; Nørskov, J. K.; Luntz, A. C. Twin Problems of Interfacial Carbonate Formation in Nonaqueous Li–O_2 Batteries. *J. Phys. Chem. Lett.* **2012**, *3*, 997–1001.

(24) McCloskey, B. D.; Bethune, D. S.; Shelby, R. M.; Mori, T.; Scheffler, R.; Speidel, A.; Sherwood, M.; Luntz, A. C. Limitations in Rechargeability of Li–O_2 Batteries and Possible Origins. *J. Phys. Chem. Lett.* **2012**, *3*, 3043–3047.

(25) Mitchell, R. R.; Gallant, B. M.; Shao-Horn, Y.; Thompson, C. V. Mechanisms of Morphological Evolution of Li_2O_2 Particles During Electrochemical Growth. *J. Phys. Chem. Lett.* **2013**, *4*, 1060–1064.

(26) Débart, A.; Bao, J.; Armstrong, G.; Bruce, P. G. An O_2 Cathode for Rechargeable Lithium Batteries: The Effect of a Catalyst. *J. Power Sources* **2007**, *174*, 1177–1182.

(27) Lu, Y.-C.; Gasteiger, H. a.; Parent, M. C.; Chiloyan, V.; Shao-Horn, Y. The Influence of Catalysts on Discharge and Charge Voltages of Rechargeable Li–Oxygen Batteries. *Electrochem. Solid-State Lett.* **2010**, *13*, A69.

(28) Shao, Y.; Park, S.; Xiao, J.; Zhang, J.; Wang, Y.; Liu, J. Electrocatalysts for Nonaqueous Lithium–Air Batteries: Status, Challenges, and Perspective. *ACS Catal.* **2012**, *2*, 844–857.

(29) Oh, S. H.; Nazar, L. F. Oxide Catalysts for Rechargeable High-Capacity Li–O_2 Batteries. *Adv. Energy Mater.* **2012**, *2*, 903–910.

(30) McCloskey, B. D.; Scheffler, R.; Speidel, A.; Bethune, D. S.; Shelby, R. M.; Luntz, A. C. On the Efficacy of Electrocatalysis in Nonaqueous Li–O_2 Batteries. *J. Am. Chem. Soc.* **2011**, *133*, 18038–41.

(31) Freunberger, S. a; Chen, Y.; Drewett, N. E.; Hardwick, L. J.; Bardé, F.; Bruce, P. G. The Lithium–Oxygen Battery with Ether-Based Electrolytes. *Angew. Chem., Int. Ed. Engl.* **2011**, *50*, 8609–13.

(32) Lim, H.; Yilmaz, E.; Byon, H. R. Real-Time XRD Studies of Li–O_2 Electrochemical Reaction in Nonaqueous Lithium–Oxygen Battery. *J. Phys. Chem. Lett.* **2012**, *3*, 3210–3215.

(33) Leskes, M.; Drewett, N. E.; Hardwick, L. J.; Bruce, P. G.; Goward, G. R.; Grey, C. P. Direct Detection of Discharge Products in Lithium–Oxygen Batteries by Solid-State NMR Spectroscopy. *Angew. Chem., Int. Ed. Engl.* **2012**, *51*, 8560–3.

(34) Xu, Z.; Stebbins, J. F. ^6Li Nuclear Magnetic Resonance Chemical Shifts, Coordination Number and Relaxation in Crystalline and Glassy Silicates. *Solid State Nucl. Magn. Reson.* **1995**, *5*, 103–12.

(35) Xiao, J.; Hu, J.; Wang, D.; Hu, D.; Xu, W.; Graff, G. L.; Nie, Z.; Liu, J.; Zhang, J.-G. Investigation of the Rechargeability of Li–O_2 Batteries in Non-Aqueous Electrolyte. *J. Power Sources* **2011**, *196*, 5674–5678.

(36) Huff, L. A.; Rapp, J. L.; Zhu, L.; Gewirth, A. A. Identifying Lithium−Air Battery Discharge Products through ^{6}Li Solid-State MAS and ^{1}H−^{13}C Solution NMR Spectroscopy. *J. Power Sources* **2013**, *235*, 87−94.
(37) Abys, J. A.; Barnes, D. M.; Feller, S.; Rouse, G. B.; Risen, W. M., Jr. Preparation of O^{17}-Labelled Glasses and Glass Precursers. *Mater. Res. Bull.* **1980**, *15*, 1581−1587.
(38) Massiot, D.; Fayon, F.; Capron, M.; King, I.; Le Calv, S.; Alonso, B.; Durand, J.-O.; Bujoli, B.; Gan, Z.; Hoatson, G. Modelling One- and Two-Dimensional Solid-State NMR Spectra. *Magn. Reson. Chem.* **2002**, *40*, 70−76.
(39) Bennett, A. E.; Griffin, R. G.; Ok, J. H.; Vega, S. Chemical Shift Correlation Spectroscopy in Rotating Solids: Radio Frequency-Driven Dipolar Recoupling and Longitudinal Exchange. *J. Chem. Phys.* **1992**, *96*, 8624.
(40) Veshtort, M.; Griffin, R. G. SPINEVOLUTION: A Powerful Tool for the Simulation of Solid and Liquid State NMR Experiments. *J. Magn. Reson.* **2006**, *178*, 248−282.
(41) Wu, G. Solid-State ^{17}O NMR Studies of Organic and Biological Molecules. *Prog. Nucl. Magn. Reson. Spectrosc.* **2008**, *52*, 118−169.
(42) Laoire, C. O.; Mukerjee, S.; Plichta, E. J.; Hendrickson, M. a.; Abraham, K. M. Rechargeable Lithium/TEGDME-$LiPF_6$/O_2 Battery. *J. Electrochem. Soc.* **2011**, *158*, A302.
(43) Dunstan M. T.; Griffin J. M. ; Blanc F.; Leskes M.; Grey C. P. Lithium Ion Dynamics in Li_2CO_3 Studied by Solid State NMR and First Principles Calculations. *In Preparation*.
(44) Oh, S. H.; Black, R.; Pomerantseva, E.; Lee, J.; Nazar, L. F. Synthesis of a Metallic Mesoporous Pyrochlore as a Catalyst for Lithium−O_2 Batteries. *Nat. Chem.* **2012**, *4*, 1004−10.
(45) Meini, S.; Tsiouvaras, N.; Schwenke, K. U.; Piana, M.; Beyer, H.; Lange, L.; Gasteiger, H. A. Rechargeability of Li−Air Cathodes Pre-filled with Discharge Products Using an Ether-Based Electrolyte Solution: Implications for Cycle-Life of Li−Air Cells. *Phys. Chem. Chem. Phys.* **2013**, 11478−11493.
(46) Stejskal, E. .; Schaefer, J.; Waugh, J. . Magic-Angle Spinning and Polarization Transfer in Proton-Enhanced NMR. *J. Magn. Reson.* **1977**, *28*, 105−112.
(47) Wang, H.; Xie, K. Investigation of Oxygen Reduction Chemistry in Ether and Carbonate Based Electrolytes for Li−O_2 Batteries. *Electrochim. Acta* **2012**, *64*, 29−34.
(48) Sharon, D.; Etacheri, V.; Garsuch, A.; Afri, M.; Frimer, A. a.; Aurbach, D. On the Challenge of Electrolyte Solutions for Li−Air Batteries: Monitoring Oxygen Reduction and Related Reactions in Polyether Solutions by Spectroscopy and EQCM. *J. Phys. Chem. Lett.* **2013**, *4*, 127−131.
(49) Assary, R. S.; Lau, K. C.; Amine, K.; Sun, Y.-K.; Curtiss, L. A. Interactions of Dimethoxy Ethane with Li_2O_2 Clusters and Likely Decomposition Mechanisms for Li−O_2 Batteries. *J. Phys. Chem. C* **2013**, *117*, 8041−8049.
(50) Hardwick, L. J.; Bruce, P. G. The Pursuit of Rechargeable Non-Aqueous Lithium−Oxygen Battery Cathodes. *Curr. Opin. Solid State Mater. Sci.* **2012**, *16*, 178−185.
(51) Bryantsev, V. S.; Uddin, J.; Giordani, V.; Walker, W.; Addison, D.; Chase, G. V. The Identification of Stable Solvents for Nonaqueous Rechargeable Li−Air Batteries. *J. Electrochem. Soc.* **2012**, *160*, A160−A171.
(52) Bryantsev, V. S.; Faglioni, F. Predicting Autoxidation Stability of Ether- and Amide-Based Electrolyte Solvents for Li−Air Batteries. *J. Phys. Chem. A* **2012**, *116*, 7128−38.
(53) Assary, R. S.; Lau, K. C.; Amine, K.; Sun, Y.-K.; Curtiss, L. a. Interactions of Dimethoxy Ethane with Li_2O_2 Clusters and Likely Decomposition Mechanisms for Li−O_2 Batteries. *J. Phys. Chem. C* **2013**, *117*, 8041−8049.
(54) Bryantsev, V. S.; Blanco, M. Computational Study of the Mechanisms of Superoxide-Induced Decomposition of Organic Carbonate-Based Electrolytes. *J. Phys. Chem. Lett.* **2011**, *2*, 379−383.
(55) Lau, K. C.; Assary, R. S.; Redfern, P.; Greeley, J.; Curtiss, L. A. Electronic Structure of Lithium Peroxide Clusters and Relevance to Lithium−Air Batteries. *J. Phys. Chem. C* **2012**, *116*, 23890−23896.